Received: 17 February 2021 | Revised: 29 June 2021

DOI: 10.1111/sapm.12439

STUDIES IN APPLIED MATHEMATICS WILEY

ORIGINAL ARTICLE

Language competition on lattices

Todd Kapitula[1] | **Panayotis G. Kevrekidis**[2]

[1] Department of Mathematics and Statistics, Calvin University, Grand Rapids Michigan, USA

[2] Department of Mathematics and Statistics, University of Massachusetts, Amherst Massachusetts, USA

Correspondence
Todd Kapitula, Department of Mathematics and Statistics, Calvin University, Grand Rapids, MI 49546, USA.
Email: tmk5@calvin.edu

Abstract

We consider a language dynamics ODE model for two languages on a square lattice. The model is an extension of the one popularized by Abrams and Strogatz. In our study, we are interested in the existence and spectral stability of structures such as stripes, which are realized through pulses and/or the concatenation of fronts, and spots, which are a contiguous collection of sites in which one language is dominant. Because the coupling between adjacent sites is nonlinear, the transition between regions speaking two different languages is super-exponential. The full dynamics are considered as a function of the prestige of a language. It is seen that as the prestige varies, it allows for a language to spread through the lattice, or conversely for its demise. Although most of the work is done assuming a square lattice, we briefly consider the problem on a triangle lattice to illustrate the robustness of the findings. We conclude by looking at the existence and spectral stability of fronts and pulses for an associated continuum PDE model. In this model, the super-exponential decay associated with the lattice model is reflected in the existence of compactly supported structures (compactons).

KEYWORDS
language competition, ODE bifurcation theory

1 | INTRODUCTION

In their seminal paper,[1] Abrams and Strogatz developed a simple ODE model,

$$\dot{u} = (1-u)u^p - Au(1-u)^p, \tag{1}$$

to help understand language competition and the decline in the number of people who speak such historic languages as Welsh, Quechua, and Scottish Gaelic. We will henceforth label Equation (1) as the AS model (see Figure 1 for a cartoon representation of this compartment model). The underlying assumptions for this model are that all speakers are monolingual, and the population is highly connected with no spatial or social structure. In Equation (1), u represents the proportion of the population that speak language U. If v is the proportion that speak language V, as all speakers are monolingual, $v = 1-u$. The assumption of monolingual speakers only may be considered to be too simplistic in terms of language; however, in the context of religious affiliation, it is natural, as here language U actually refers to those who have some type of religious affiliation, and language V represents those who do not.[2]

The parameter $p > 0$ measures *volatility*. The case $p = 1$ is a neutral situation, where transition probabilities from one language to another depend linearly on local language densities. If $p > 1$, there is a larger than neutral resistance to changing the language (low volatility), and if $p < 1$, there is a lower than neutral resistance to changing the language (high volatility). Experimentally, it is estimated that $p = 1.31 \pm 0.25$.[1] In this paper, we respect the experimental findings and assume $p > 1$, so the volatility is low.

The parameter $A > 0$ represents the affinity of the general population towards one language or the other. In linguistics terminology, the parameter A can be used to represent the *prestige* associated with a particular language. The fixed points $u = 0$ (language V is preferred) and $u = 1$ (language U is preferred) are stable, while $u = B/(1+B)$ with $B = A^{1/(p-1)}$ is unstable. If $A < 1$ and $u(0) = 0.5$ (both languages are initially equally preferred), then $u(t) \to 1$ as $t \to +\infty$, so the population has an affinity for language U or language U has more prestige in the general population. On the other hand, if $A > 1$ and $u(0) = 0.5$, then $u(t) \to 0$ as $t \to +\infty$, so language V has more prestige in the entire population.

An agent-based model associated with the AS model Equation (1) when $p = 1$,

$$\dot{u} = (1-A)u(1-u), \tag{2}$$

is considered in Ref. 30. In the derivation of this continuum model it is assumed, for example, on a square lattice, that an individual interacts only with the nearest neighbors. When $A \neq 1$, the agent-based model gives the same interpretation as (2). In particular, if U has more prestige, then the entire population will eventually speak language U, whereas if V has more prestige, then all will eventually speak language V. An agent-based model is also considered in Ref. 32. In the fully connected case, the dynamics of the associated mean-field model are equivalent to the AS model.

As pointed out by Ref. 22, the monolingual assumption implies the two languages are so dissimilar that conversation is practically impossible between the two competing language groups. These authors extend the AS model to allow for languages that are similar enough for there to be bilingual speakers. The proportion of the population that is bilingual satisfies $b = 1-u-v$ with

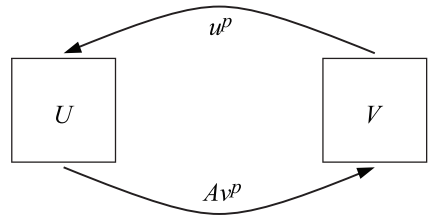

FIGURE 1 The compartment model associated with AS model Equation (1). The variable u represents the proportion of the population that speaks language U, and v is the proportion that speaks language V. It is assumed $u + v = 1$

$0 \leq b \leq 1$. The model is

$$\begin{aligned} \dot{u} &= (1-k)(1-u)(1-v)^p - Au(1-u)^p \\ \dot{v} &= (1-k)A(1-v)(1-u)^p - v(1-v)^p, \end{aligned} \tag{3}$$

where $0 < k < 1$ represents the ease of bilingualism. In particular, $k = 0$ means that conversation is not possible between monolingual speakers, and $k = 1$ implies $U = V$. The larger the value of k, the more similar are the two languages. If $k = b = 0$, then model Equation (3) reduces to model Equation (1). An analysis of the model Equation (3) is provided in Refs. 8, 9, 25.

The AS model has been extended to networks. Each node of the network corresponds to a group whose dynamics are governed by the AS model, while the dynamics between groups satisfy some other rule. Amano et al.[3] collected and analyzed world-wide data taking into account such things as geographical range size, speaker population size, and speaker growth rate (i.e., changes in the number of speakers) of the world's languages, and assessed interrelations among these three components to understand how they contribute to shaping extinction risk in languages. The role of population density and how it effects the interaction rates among groups is discussed in Ref. 18 in the context of language shift in Galicia, which is a bilingual community in northwest Spain. They model the problem by looking at Equations (3) on a network, with the strength of the interactions between nodes depending on the population density. The model for $j = 1, \ldots, n$ is

$$\begin{aligned} \dot{u}_j &= (1-k_j)(1-u_j)(1-v_j)^p - A_j u_j (1-u_j)^p + K_j\left(\overline{u} - u_j\right) \\ \dot{v}_j &= (1-k_j)A_j(1-v_j)(1-u_j)^p - v_j(1-v_j)^p + K_j\left(\overline{v} - v_j\right). \end{aligned} \tag{4}$$

Here $\overline{y}$ represents the average of the set, $\{y_j\}$. The positive parameter K_j is assumed to be a strictly increasing function of the population density. The authors[33] follow a similar strategy, except they assume the nonlinearities are of Lotka–Volterra type. Taking a different approach, Ref. 35 assume a diffusion process to take into account spatial effects. Fujie et al.[13] and Zhou et al.[36] consider the problem of competition among more than two languages.

In this paper, we consider the language competition problem on lattices under the assumption of low volatility, $p > 1$. For ease, we will primarily work with $p = 2$, but our experience is that other values of $p > 1$ do not affect the results qualitatively. As long as the interactions are superlinear, the relevant phenomenology and associated bifurcation diagrams do not change significantly as regards their principal features. We will assume there is no bilingual subpopulation (see Refs. 18, 23, 25 for some work in this area under the assumption of a single group). We will

assume the existence of n distinct population groups, and let $0 \leq u_j \leq 1$ represent the proportion of those in group j who speak language U ($v_j = 1 - u_j$ speak language V). For each $j = 1, \dots, n$, the resulting equation is a natural extension of the compartment model illustrated in (1),

$$\dot{u}_j = \left(\sum_{k=1}^{n} \boldsymbol{I}_{jk} u_k^p \right) \cdot (1 - u_j) - A_j \left(\sum_{k=1}^{n} \boldsymbol{I}_{jk} (1 - u_k)^p \right) \cdot u_j, \tag{5}$$

where $\boldsymbol{I}_{jk} \geq 0$. We implicitly assume in this model that the population of each group is fixed, and there is no migration of speakers from one group to another. We call the matrix $\boldsymbol{I} = (\boldsymbol{I}_{jk})$ the influence matrix, and the term $\boldsymbol{I}_{jk}$ represents the influence group k has on group j through the between-group reaction rate. If we think of the system (5) as being a compartment model, then the term $\boldsymbol{I}_{jk} u_k^p$ is the rate constant associated with the influence that the U speakers in group k have on the V speakers in group j, and $\boldsymbol{I}_{jk}(1 - u_k)^p$ is the rate constant associated with the influence that the V speakers in group k have on the U speakers in group j. Clearly, when $n = 1$, the system (5) collapses to the AS model Equation (1). Later in this paper, we will look at the dynamics associated only with specific influence matrices; namely, that associated with a square lattice in 3 and 4, and that for a triangular lattice in 5.

Let us briefly compare the systems (4) and (5). In the case of no bilingual speakers, the system (4) collapses to

$$\dot{u}_j = (1 - u_j) u_j^p - A_j u_j (1 - u_j)^p + K_j \left(\overline{u} - u_j \right). \tag{6}$$

First note that the systems (5) and (6) have the feature that the on-site dynamics are the same as those for the AS model. The model Equation (6) has a linear coupling term that assumes group j is influenced by the difference between the average proportion of language U speakers for all the groups and the proportion who speak U in group j. On the other hand, under the assumption that each external group has an equal influence on a given group, $\boldsymbol{I}_{jj} = 1$ and $\boldsymbol{I}_{jk} = K_j/(n-1)$ for all $k \neq j$, the system (5) becomes

$$\dot{u}_j = (1 - u_j) u_j^p - A_j u_j (1 - u_j)^p + K_j \left[(1 - u_j) \overline{u_{\neq j}^p} - A_j u_j \overline{(1 - u)_{\neq j}^p} \right], \tag{7}$$

where we use the notation,

$$\overline{f_{\neq j}} = \frac{1}{n-1} \sum_{k \neq j} f_k.$$

The nonlinear coupling term for the model Equation (7) takes into account the average proportion of speakers of language U and language V for all other groups, and is clearly very different from the linear coupling term associated with the model Equation (6). It is an open question as to whether this functional difference in the coupling terms leads to a qualitative difference in the dynamics.

The AS model can also be used to model opinion propagation in a population in which it is assumed that people have either opinion U, or opinion V, where we think of V as being "not U." Marvel et al.,[21] hereafter referred to as MS, provide a model similar to (3) in which it is assumed there are three distinct groups: those who hold opinion U, those who hold opinion V, and the

remaining who are undecided,

$$\dot{u} = (1 - u - v)u - uv$$

$$\dot{v} = (1 - u - v)v - uv.$$

The underlying assumption in this compartment model is that in order for one who initially holds opinion U to eventually hold opinion V (or vice-versa), the person first must become undecided. Wang et al.[34] extended the MS model to allow for several competing opinions. The MS model was extended to networks in Ref. 7, and this extended model was studied using dynamical systems techniques. Tanabe and Masuda[31] proposed and analyzed an interesting opinion formation model (hereafter labelled TM) in which it was assumed that the population itself breaks down into two groups: congregators and contrarians. In contrast, the MS model implicitly assumes the entire population is filled with congregators. One conclusion of the TM model is that if a large enough proportion of the population is contrarian, then no majority opinion will be achieved. This is in contrast to the conclusion of those models in which it is assumed there are only congregators, as here a majority opinion is always obtained. The TM model was later refined in Ref. 11, and the new model allowed for the effects of peer pressure, and incorporated the influence of zealots. From a qualitative perspective, the mean-field models used for opinion dynamics and language death have many similarities. Thus, although we frame our results using the formulation associated with language, they are also directly applicable to mean-field opinion formation models.

In this paper, we are primarily interested in the existence and stability of spatial structures for the network system (5). For the sake of exposition, we mostly assume the groups have been arranged on a square lattice, so u_{jk} will represent the proportion of the population at site (j, k) who speak language U. We will also briefly consider a triangular lattice to demonstrate that the lattice type does not appear to have a large qualitative influence on the dynamics. The interactions on the lattice are nearest-neighbor (NN) only, and there will be no preferential distinction in the reaction rates, $\boldsymbol{I}_{jk} = \boldsymbol{I}_{kj}$. We will also assume the prestige is uniform throughout the entire lattice, $A_{jk} = A$. Even under the assumption on the interaction matrix, it is an interesting problem in its own right to allow for a spatially inhomogeneous distribution of the prestige and see how it affects the prevalent dynamics. The consequences of removing these assumptions will be left for a future paper.

For the square lattice, we start by considering the existence and stability of fronts and pulses for the system (5), as these are prototypical nonlinear patterns that may mediate the spread of a language, opinion, or religious affiliation over the lattice domain of interest. The underlying assumption here is $u_{jk} = U_j$, so the 2D problem becomes an effectively 1D problem. A front is a solution for which $U_j = 0$ (or $U_j = 1$) for $1 \leq j \leq n_0$, and $U_j = 1$ (or $U_j = 0$) for $j \geq n_0 + \ell$ and some $\ell \geq 1$. In other words, to the left of n_0 language V is spoken, and to the right of $n_0 + \ell$ language U is spoken. For the 1D problem, a pulse is a solution for which $U_j = 0$ for $j \leq n_0$ and $j \geq n_0 + \ell$, and $U_j > 0$ for $n_0 < j < n_0 + \ell$. On the full lattice, a pulse solution in what follows will correspond to a stripe of language U speakers who are surrounded on both sides by V speakers. We will consider when fronts can travel, which implies that language U is invading language V, or vice-versa. We will also consider when pulses can grow or shrink. We will see that a growing pulse can be thought of as the concatenation of two fronts traveling in opposing directions, so language U eventually takes over the entire lattice. A shrinking pulse eventually disappears, which means that language U has gone extinct. As we will see, the prestige associated with speaking U ($A < 1$) or V ($A > 1$) plays a central role in the analysis. We will also briefly look at a fully 2D structure, a

spot, which is a contiguous group of sites with $u_{jk} > 0$ surrounded by $u_{jk} = 0$—an island of U in a sea of V. We will briefly redo the analysis for a triangular lattice to demonstrate that the lattice type does not appear to be important from a qualitative perspective. Of course, it is an open problem to show that this is actually the case. We will conclude by looking at the associated continuum model, and study the existence and spectral stability of (concatenated) waves for this model. Here the nonlinear diffusion allows for compactly supported spatial structures, which actually makes it easier to study concatenated waves because of the absence of tail–tail interactions.

2 | THE MODEL ON A SQUARE LATTICE

We consider the model Equation (5) on a square lattice with NN interactions only. The prestige will be uniform throughout the lattice, $A_{jk} = A$. Although we will assume $p = 2$, our numerical experiments indicate that from a qualitative perspective the results presented herein are robust as long as $p > 1$. Under these assumptions, the model Equation (5) is

$$\begin{aligned}\dot{u}_{jk} = &\Big[\epsilon_0 u_{jk}^2 + \epsilon_1\Big(u_{j+1,k}^2 + u_{j-1,k}^2 + u_{j,k+1}^2 + u_{j,k-1}^2\Big)\Big](1-u_{jk})\\ &- A\big[\epsilon_0(1-u_{jk})^2 + \epsilon_1\big((1-u_{j+1,k})^2 + (1-u_{j-1,k})^2 + (1-u_{j,k+1})^2 + (1-u_{j,k-1})^2\big)\big]u_{jk}.\end{aligned}$$

Here $1 \le j,k \le n$, and we assume in the model that at the edge of the square there are Neumann boundary conditions, for example, $u_{n+1,k} = u_{nk}$. The parameter $\epsilon_0 > 0$ is the on-site interaction rate, and the parameter $\epsilon_1 > 0$ is the NN interaction rate. Using the notation for the discrete Laplacian,

$$\Delta_{\text{dis}} f_{jk} = f_{j+1,k} + f_{j-1,k} + f_{j,k+1} + f_{j,k-1} - 4f_{jk},$$

the ODE takes the more compact form,

$$\begin{aligned}\dot{u}_{jk} = &(\epsilon_0 + 4\epsilon_1)u_{jk}(1-u_{jk})\big[(1+A)u_{jk} - A\big] + 2A\epsilon_1 u_{jk}\Delta_{\text{dis}} u_{jk}\\ &+ \epsilon_1\big[1-(1+A)u_{jk}\big]\Delta_{\text{dis}} u_{jk}^2.\end{aligned} \tag{8}$$

Note that in this formulation the onsite interaction rate is also influenced by the NN interaction rate.

If we assume that the interactions between neighbors are strong, $\epsilon_1 \gg 1$, then on setting $R = \epsilon_0 + 4\epsilon_1 \gg 1$, we have the limiting continuum model,

$$\partial_t u = Ru(1-u)[(1+A)u - A] + (1+A)u(1-u)\Delta u + [1-(1+A)u]|\nabla u|^2. \tag{9}$$

Here Δ represents the Laplacian, and ∇ is the gradient operator. The continuum model incorporates the expected temporal dynamics associated with the original ODE model, but the coupling dynamics between sites is dictated by an effective nonlinear diffusion. The PDE is physical in the following sense: $u(x,y,t) = 0$ implies $\partial_t u(x,y,t) \ge 0$, and $u(x,y,t) = 1$ implies $\partial_t u(x,y,t) \le 0$. Note that diffusion is not present when the entire population supports one language, $u = 0$ or $u = 1$. This is the underlying mechanism associated with compactly supported steady-state solutions.

When studying the solution structure to the ODE (8), or the accompanying PDE (9), we will first focus on the existence and spectral stability of time-independent patterns that vary in one direction only. For the ODE (8), we will set $u_{j,k}(t) = U_j$ for all j, k, and U_j will solve the 1D discrete model,

$$0 = (\epsilon_0 + 4\epsilon_1)U_j(1-U_j)\big[(1+A)U_j - A\big] + 2\epsilon_1 A U_j \Delta_j U_j + \epsilon_1\big[1-(1+A)U_j\big]\Delta_j U_j^2, \tag{10}$$

where $\Delta_j f_j = f_{j+1} + f_{j-1} - 2f_j$. For the PDE (9), we will set $u(x,y,t) = U(x)$, and $U(x)$ will solve the nonlinear ODE,

$$0 = RU(1-U)[(1+A)U - A] + (1+A)U(1-U)U'' + [1-(1+A)U](U')^2, \quad ' = \frac{\mathrm{d}}{\mathrm{d}x}. \tag{11}$$

In both cases, we will be looking for fronts and pulses, the latter of which corresponds to stripes for the full system. These solutions act as transitions between regions where language U is dominant and language V is dominant.

Remark 1. Even though the derivation is dissimilar, the continuum model Equation (9) is remarkably similar to the mean-field model associated with the square lattice as provided for in Ref. [32, equation (48)]. The model Equation (9) has the additional term, $[1-(1+A)u]|\nabla u|^2$; however, both models have the important feature that the diffusion coefficient is singular. Dynamically, both systems have the feature that a contiguous domain tends to evolve in a way that reduces the curvature of the boundary (see also further relevant discussion regarding the dynamics below).

3 | EXISTENCE AND SPECTRAL STABILITY OF STRIPES FOR THE DISCRETE MODEL

A front solution to the discrete model Equation (10) satisfies $U_j = 0\,(1)$ for $j \leq \ell$, and $U_j = 1\,(0)$ for $j \geq k$, where $1 < \ell < k < n$. A pulse solution will satisfy $U_j = 0\,(1)$ for $j \leq \ell$ and $j \geq k$, and $U_j \sim 1\,(0)$ for $\ell < j < k$. The transition between the states 0 and 1 will be monotone. A stripe solution to the full 2D model will be a pulse, or a concatenation of two fronts. As we will see, the concatenation of two fronts provides for a "thicker" stripe. In the same spirit, we can also discuss multi-stripes, which are the concatenation of several pulses and/or fronts.

3.1 | Existence: fronts

If $\epsilon_1 = 0$, the system uncouples, so a monotone front can be constructed analytically. In this limit, for a front we set $U_j = 0\,(1)$ for $j = 1, \dots, \ell$, and $U_j = 1\,(0)$ for $j = \ell+1, \dots, n$. We will refer to this front as the off-site front. As each of the fixed points is stable for the scalar AS model, the front will be stable for the full system. By the Implicit Function Theorem, the front will persist and be stable for $0 < \epsilon_1 \ll 1$. We can concatenate these fronts when $\epsilon_1 = 0$ to form stable stripes, and then again apply the Implicit Function Theorem to show the existence and stability for small ϵ_1.

When $\epsilon_1 = 0$, we can construct another monotone front by setting $U_j = 0\,(1)$ for $j = 1, \dots, \ell$, $U_{\ell+1} = A/(1+A)$, and $U_j = 1\,(0)$ for $j = \ell+2, \dots, n$. As all of the fixed points but the

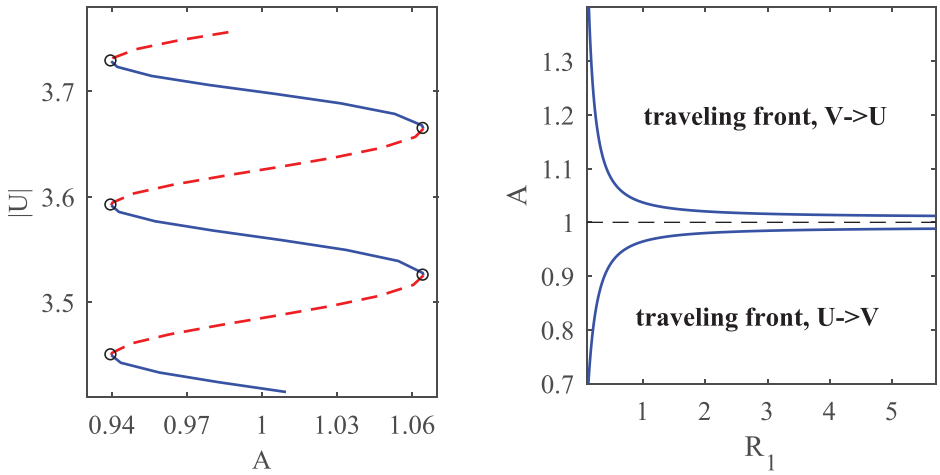

FIGURE 2 Numerically generated existence curves for stationary $V \to U$ fronts, that is, $U_j = 0$ to the left, and $U_j = 1$ to the right. The curve is given for $R_1 = 0.6$ in the left panel. The solid (blue) curves denote a stable front (when $A = 1$ it is an off-site front), and the dashed (red) curves denote an unstable front (when $A = 1$ it is an on-site front). The saddle-node bifurcation points are given by black circles. The vertical axis is the ℓ^2-norm. Regarding the boundary in the right panel, inside the two curves (which are the saddle-node bifurcation points) there is a stable stationary front, and outside the curves the front travels. The invading language is provided in the figure

one at $j = \ell$ are stable for the scalar AS model, the front will be unstable for the full system with the linearization having one positive eigenvalue. By the Implicit Function Theorem, the front will persist and be unstable with one positive eigenvalue for $0 < \epsilon_1 \ll 1$. We will refer to this front as the on-site front.

When $\epsilon_1 = 0$, the off-site and on-site fronts exist for any value of A. However, once there is nontrivial coupling we expect there will be an interval of A values that contains $A = 1$ on which the fronts will exist. In order to determine this interval, we will do numerical continuation using the MATLAB package, Matcont[10]. Using this package will also allow us to numerically continue bifurcation points in parameter space. Setting

$$R_1 = \frac{\epsilon_1}{\epsilon_0},$$

we will numerically explore the (R_1, A)-parameter space. We will use the above theoretical results as a starting point for small R_1.

For each fixed $R_1 > 0$, there will be an associated snaking diagram in the parameter A. For a particular example, consider the left figure in Figure 2. The horizontal axis is A, and the vertical axis is the ℓ^2-norm of the front. In this figure, the solid (blue) curve corresponds to a stable front (which is off-site when $A = 1$), and the dashed (red) curve corresponds to an unstable front (which is on-site when $A = 1$). These two curves meet at a saddle-node bifurcation point, which is denoted by an open black circle. We see there is an $A_- < 1 < A_+$ for which there are stable fronts when $A_- < A < A_+$, and no stationary fronts (at least as seen via numerical continuation) outside this interval. The values of $A_\pm$ depend on R_1. Each of the upward shifts of the stable and unstable branches correspond to waveforms that are shifted by an integer number of lattice nodes to the left (hence the growth in norm). The right panel in 2 shows the functions $A_\pm$ as a function of R_1. Althtough we do not show it here, even in the limit $R_1 \to +\infty$ the two curves do not converge to

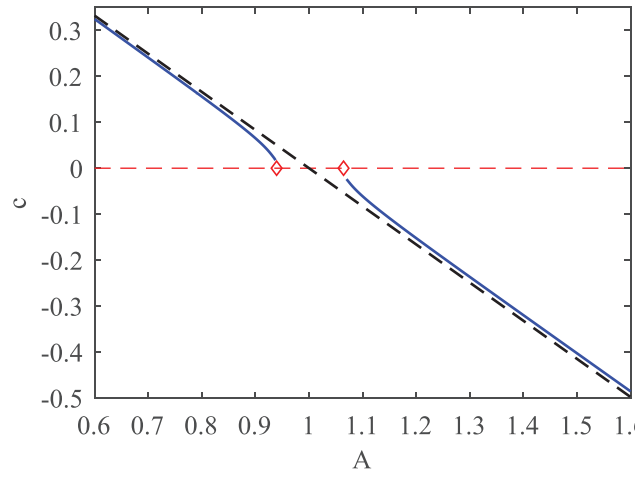

FIGURE 3 The numerically generated wave speed when $R_1 = 0.6$ is given by the solid (blue) curve. The (red) diamonds mark the boundary for the existence of the stationary front, $A_- \sim 0.9395$ and $A_+ \sim 1.0644$, at which the wave speed is zero. The dashed black line is the wave-speed prediction of Equation (13) provided by the PDE model

1; instead, we have $A_+(+\infty) \sim 1.0082$, and $A_-(+\infty) \sim 0.9918$. Inside the two curves, and for fixed R_1, there is a stable stationary front.

3.2 | Existence: traveling fronts

Outside the two curves, $A_\pm(R_1)$, there is a traveling front. Traveling waves will be written as $U(x + ct)$, so $U_j(t) = U(j + ct)$. Setting $\xi = x + ct$, the resulting forward–backward difference equation to which the traveling wave is a solution is

$$\begin{aligned} cU' = {} & (\epsilon_0 + 4\epsilon_1)U(1-U)[(1+A)U - A] \\ & + 2A\epsilon_1 U[U(\xi+1) + U(\xi-1) - 2U(\xi)] \\ & + \epsilon_1[1-(1+A)U]\left[U(\xi+1)^2 + U(\xi-1)^2 - 2U(\xi)^2\right]. \end{aligned}$$

This system is numerically solved using a variant of Newton's method (see Refs. 12, 15, 17 for the details).

We consider in detail the case of $R_1 = 0.6$. The numerical result is plotted in Figure 3. Our experience is that from a qualitative perspective the value of R_1 is not particularly important, as diagrams similar to Figure 3 can be obtained for different values of R_1. The points $A_\pm(R_1)$ are marked with a (red) diamond. It should be the case that at these points $c = 0$; unfortunately, the fact that the linearization becomes singular at $A = A_\pm$ precludes good convergence of the algorithm near these points. Away from these bifurcation points there is good convergence of the numerical algorithm. Assuming $U_j = 0$ to the left, and $V_j = 0$ to the right,

- $c < 0$ means language V invades language U
- $c > 0$ means language U invades language V.

From the simulation we see that if $A > A_+ \sim 1.0644$, that is, language V has more prestige, then language V invades language U. On the other hand, if $A < A_- \sim 0.9395$, that is, language U has more prestige, then language U invades language V. Note that the speed increases as the preferred language becomes more prestigious. Indeed, up to a small correction, and sufficiently far away

from $A_\pm$, the wave speed follows the formal prediction of the continuum model, Equation (13). The predicted curve, which is associated with the limit $R_1 \to +\infty$, is given by the black dashed line. This result has been numerically verified for several different values of R_1. One can observe the nontrivial effect of discreteness in establishing an interval where the fronts can be stationary. Indeed, the continuum model is found to possess vanishing speed at the isolated point of prestige balance, namely at $A = 1$, while the discrete variant requires a detuning from this value in order to enable such a depinning from the vanishing speed setting.

Remark 2. It is an interesting exercise to consider the scaling law for the wave speed as $A \to A_\pm$; however, we have not pursued this. The interested reader should consult Refs. 4, 19 and the references therein for details as to how such a law may be derived.

3.3 | Existence: pulses

As is the case for fronts, if $\epsilon_1 = 0$ a pulse can be constructed analytically by setting $U_j = 0\,(1)$ for $1 \le j \le \ell$ and $k \le j \le n$, and $U_j = 1\,(0)$ for $\ell < j < k$. As each of the fixed points is stable for the scalar AS model, the pulse will be stable for the full system. By the Implicit Function Theorem, the pulse will persist and be stable for $0 < \epsilon_1 \ll 1$. We can concatenate these pulses when $\epsilon_1 = 0$ to form stable multi-pulses, and then again apply the Implicit Function Theorem to show the existence and stability for small ϵ_1. Assuming the background supports language V, the size of the pulse is the number of adjacent groups that support language U. For small ϵ_1, the size is $k - \ell - 1$.

Numerically it is seen that if a pulse is of size 4 or larger, then it is realized as a concatenation of a $V \to U$ and a $U \to V$ stationary front. Consequently, in this case the front dynamics completely determine the pulse dynamics. If the front is stationary, so is the pulse. If the front moves, so will the edge of the pulse. On the other hand, if the pulse is of size 1, 2, or 3 (see the right panels of Figure 4 for representative illustrations), then the dynamics are not related to front dynamics. From a dynamics perspective the pulse ceases to exist after a saddle-node bifurcation occurs.

Using Matcont, the saddle-node bifurcation point can be traced in (R_1, A)-space. The results are presented in Figure 4. The pulse will exist inside the boundary curve. The cusp point is $(R_1, A) \sim (0.1996, 0.6936)$ for the pulse of size 1, and $(R_1, A) \sim (0.6352, 0.9246)$ for the pulse of size 2. For a pulse of size 3, the cusp point satisfies $R_1 > 31.77$ with $0 < 1 - A \ll 1$, and is not shown in the figure. Note that the cusp point converges to $A = 1$ as the size of the pulse increases, and satisfies $A < 1$. This is due to the fact that language U has more prestige for $A < 1$. If the background was language U instead of language V, then the cusp point would satisfy $A > 1$.

From a dynamics perspective, if R_1 is less than the cusp point value, and if A is small enough so that (R_1, A) is below the bottom boundary curve, then the pulse will grow until it can be thought of as a concatenation of two fronts. Once this occurs, the edges of the pulse will move according to the front dynamics. The pulse grows because the prestige for language U is sufficiently large. On the other hand, if (R_1, A) is above the top boundary curve, then language V has sufficient prestige so that the background language prevails, and the pulse simply disappears in finite time. See Figure 5 for the corroborating results of a particular simulation; in particular, the top two panels look at a pulse of size 1, and the bottom two panels look at a pulse of size 2.

Remark 3. If we assume a pulse of language V sits on a background of language U, then we will get the same curves as in Figure 4. However, the dynamical interpretation leading to Figure 5 will

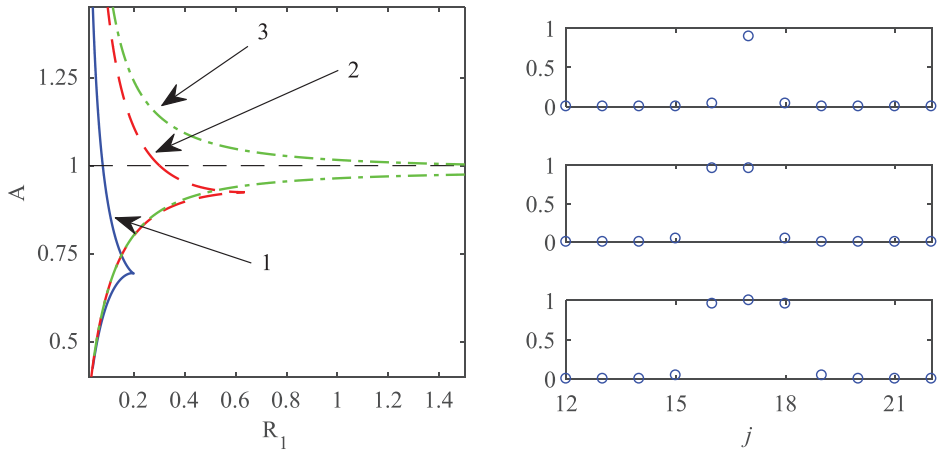

FIGURE 4 The left panel provides the numerically generated boundary of pulses of size 1 through 3. The boundary is given by a solid (blue) curve for the pulse of size 1, a (red) dashed curve for a pulse of size 2, and a (green) dashed-dotted curve for a pulse of size 3. For a given pulse size, the pulse exists inside the two curves, and ceases to exist outside. The right panel gives an example of each pulse for $R_1 = 0.05$ and $A = 1$. The pulse of size 1 is shown in the upper right panel, the pulse of size 2 in the middle right panel, and the pulse of size 3 in the lower right panel

be reversed. In particular, if A is too small the pulse will disappear, whereas if A is sufficiently large it will grow.

3.4 | Multiple stripes via pulse concatenation

We now consider the problem of concatenating individual pulses to form multi-pulses. For the sake of convenience, and without loss of generality, we assume that background consists of language V. As with the single pulses, each of the multi-pulses will be stable when $\epsilon_1 = 0$, and they will persist as stable structures for sufficiently small ϵ_1. Typically, the construction of multi-pulses would involve a discussion of tail–tail interactions between individual pulses, and an application of the Hale–Lin–Sandstede (HLS) method (e.g., see Refs 5, 6, 16, 24, 26–29 and the references therein). However, for the system under consideration this is less relevant, as the nonlinear coupling between adjacent sites renders the transition from one state to another to be super-exponential, instead of the exponential rates associated with linear coupling (see Figure 6 for a representative demonstration of this phenomena). Consequently, to leading order one can think of pulses as being compactons (a compactly supported structure), and fronts as being a compactly supported transition between two states.[1] In this light, to leading order, and as long as the individual pulses are initially sufficiently separated, the dynamics associated with a concatenation of k pulses is really just the dynamics of k uncoupled pulses, each of which evolves according to the rules presented in 3.3.

Remark 4. Unfortunately, at this time we do not know how to rigorously prove the above statements regarding the concatentation of pulses and/or fronts. The HLS method uses the linear cou-

[1] We will return to this aspect in more detail in the continuum limit analysis, see 6.1.

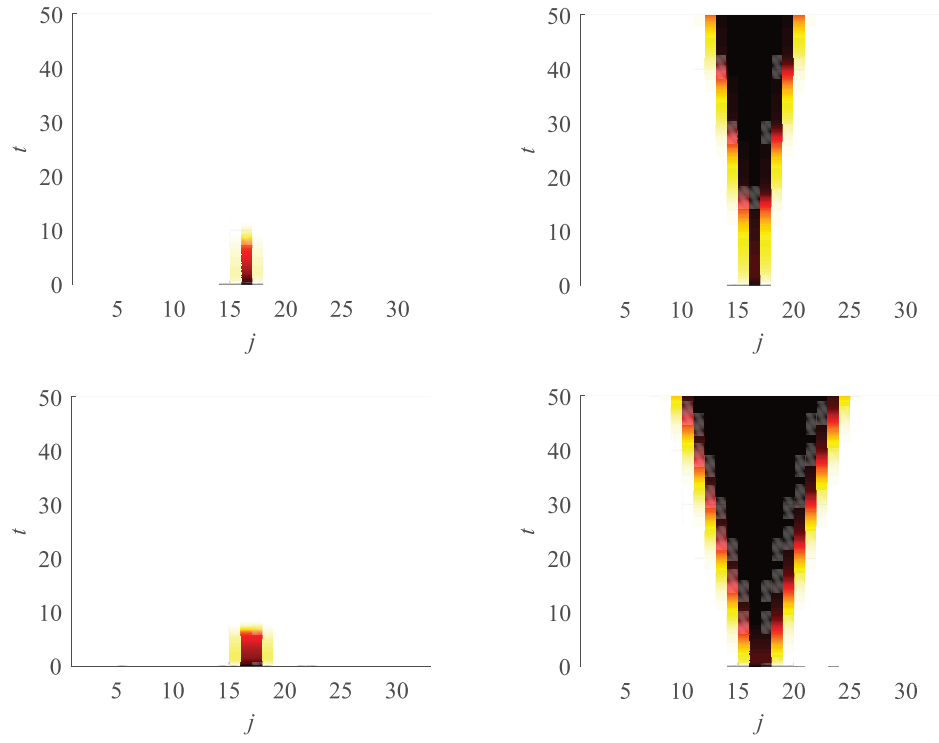

FIGURE 5 The results of a numerical simulation of the full ODE (8) where the initial condition satisfies $u_{jk}(0) = u_{j\ell}(0)$ for all k, ℓ. The color white represents language V, and the color black represents language U. In the top two figures, $R_1 = 0.15$. For the top left figure $A = 0.9$ (so the point is above the boundary for a pulse of size 1), and for the top right figure $A = 0.6$ (so the point is below the boundary for a pulse of size 1). In both figures, the initial condition for fixed k is a small perturbation of a pulse of size 1. In the bottom, two figures $R_1 = 0.5$. For the bottom left figure, $A = 1.0$ (so the point is above the boundary for a pulse of size 2), and for the bottom right figure, $A = 0.8$ (so the point is below the boundary for a pulse of size 2). In both figures, the initial condition for fixed k is a small perturbation of a pulse of size 2

pling, and the resulting exponential dichotomies, to rigorously reduce the full concatenation problem to a solvable linear algebra problem where the size of the matrix is equal to the number of concatenated pulses. At this time, it is not clear to us how to adapt the HLS methods and ideas to the problem at hand, where the coupling is both nonlinear and singular. This is clearly an interesting problem for future study.

As this is only a case study, we will focus on the example of the two-pulse, which at the $\epsilon_1 = 0$ limit we label as j-k-ℓ. Here j and ℓ refer to the size of the pulse that supports language U, and k is the intervening pulse of size k that supports language V. For example, a 2-1-2 can be thought of when $\epsilon_1 = 0$ as the sequence of u-values, $\cdots 00\mathbf{11}0\mathbf{11}00 \cdots$. Of particular interest is the value of k needed so that a two-pulse can really be thought of as the concatenation of two one-pulses.

First consider the 2-1-2 pulse. The boundary for which this solution exists (again, determined by a saddle-node bifurcation) is presented as a solid (blue) curve in Figure 7. The cusp point is $(R_1, A) \sim (0.1478, 1.2954)$. For (R_1, A) values inside the curve, the pulse will exist as a stationary solution and be stable, whereas outside the curve it does not exist. From a dynamical perspective, if $R_1 < 0.1478$, and if A is chosen so that the point lies below the lower boundary curve, then the solution will quickly become a single pulse of size 5 (i.e., the internal 0 becomes a 1), see the

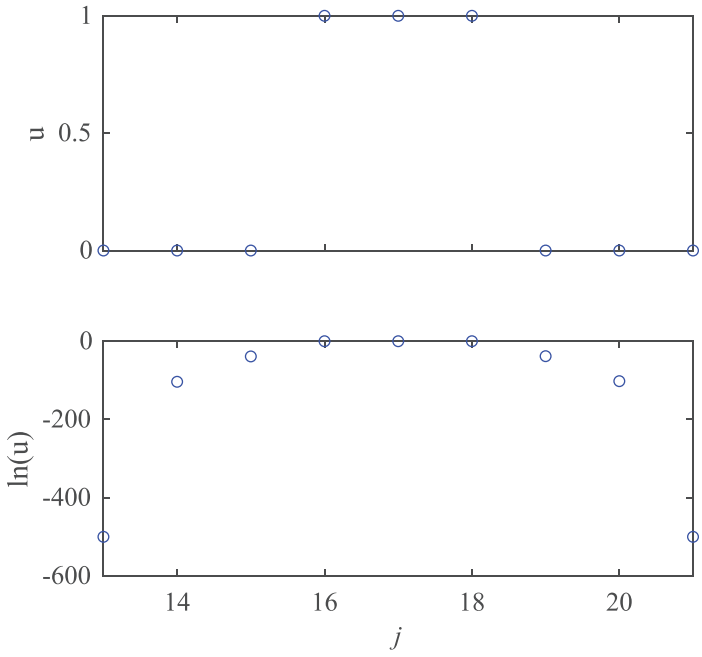

FIGURE 6 The top panel provides the numerically generated pulse of size 3, say u_3, for $(R_1, A) = (0.9, 1.0)$. The bottom panel shows $\ln(u_3)$. For $j \leq 12$ and $j \geq 22$, the numerically determined value of $\ln(u_3)$ is $-\infty$. If the decay to $u = 0$ was exponential, the bottom panel would be linear in j. Instead, it is concave down

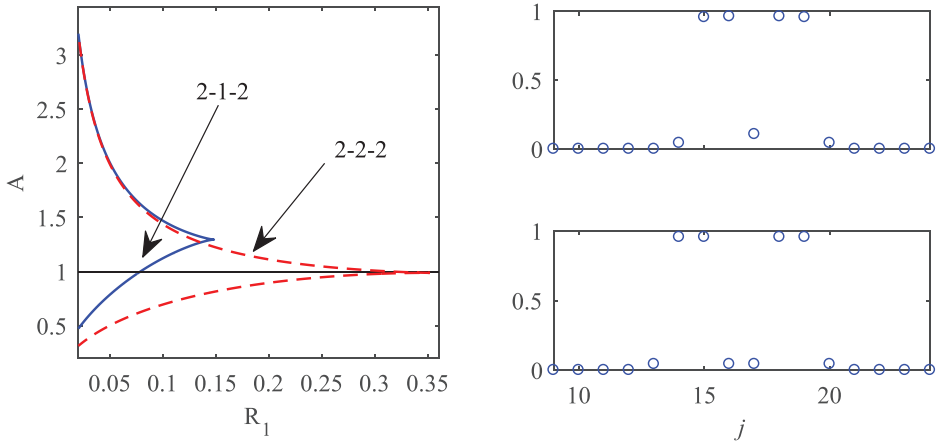

FIGURE 7 The left panel provides the numerically generated boundary of the two-pulse 2-1-2 (solid (blue) curve) and 2-2-2 (dashed (red) curve). The two-pulse exists inside the two curves, and ceases to exist outside. The right panel gives an example of each pulse when $R_1 = 0.05$ and $A = 1.0$. The 2-1-2 pulse is upper right, and the 2-2-2 pulse is lower right

center panel of Figure 8 with $(R_1, A) = (0.1, 1.0)$. As discussed previously, a pulse of this size can be thought of as the concatenation of two fronts. If the value of A is such that the point is also below the lower boundary of the curve presented in the right panel of Figure 2, so that U invades V, then both fronts will travel until the entire lattice is overtaken by language U (see the left panel of Figure 8 with $(R_1, A) = (0.1, 0.6)$). On the other hand, if $R_1 < 0.1478$, and A is chosen so that the point lies above the upper boundary curve, then the solution will quickly decay to a pulse of size zero, that is, language V is spoken over the entire lattice (see the right panel of Figure 8 with $(R_1, A) = (0.1, 1.7)$).

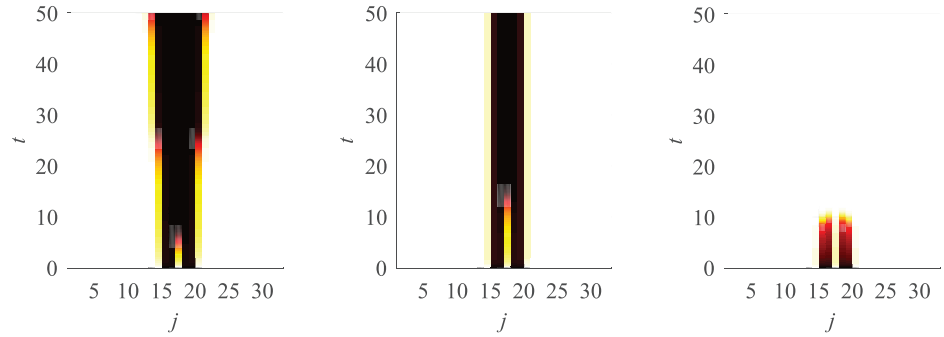

FIGURE 8 The results of a numerical simulation of the full ODE Equation (8) with $R_1 = 0.1$ where the initial condition satisfies $u_{jk}(0) = u_{j\ell}(0)$ for all k, ℓ. The color white represents language V, and the color black represents language U. In all three panels, the initial condition is a small perturbation of a 2-1-2 pulse. For the left panel $A = 0.6$, for the middle panel $A = 1.0$, and for the right panel $A = 1.7$

Remark 5. If $R_1 > 0.1478$, then the pulse no longer exists, and the fate of the perturbation is a more difficult question to answer. This task will be left for a future paper.

Next consider the 2-2-2 pulse. The boundary for which this solution exists is presented as a dashed (red) curve in Figure 7. The cusp point is $(R_1, A) \sim (0.3515, 0.9879)$. The dynamics associated with (R_1, A) points chosen outside of the domain bounded by the curve are exactly as that outlined above. For points below the curve, the solution quickly becomes a single pulse of size 6, which again is the concatenation of two fronts. Each front will travel, and U will grow, if A is sufficiently small. For points above the curve the solution again quickly decays to a pulse of size zero.

Finally, consider the 2-k-2 pulse for any $k \geq 3$. Here we find this is a true concatenation of two pulses of size 2, so the boundary curve is given by the dashed (red) curve in Figure 4. Moreover, the dynamics of this pulse is initially governed by the dynamics associated with a pulse of size 2 (see the bottom two panels of Figure 5).

Althtough we do not present the corroborating details here, there was nothing special about initially choosing $j = \ell = 2$. Consequently, we now have the following rule-of-thumb. If we start with a two-pulse of size j-k-ℓ, and if $k \geq 3$, then the resulting dynamics will initially be independently governed by those associated with the pulse of size j and pulse of size ℓ. The individual pulses "see" each other only if the gap between the two is one or two adjacent sites. Indeed, this rule holds for any concatenation of pulses. As long as the distance between adjacent pulses is at least 3 sites, the existence boundary curve is exactly that associated with each individual pulse that makes up the entire multi-pulse. Moreover, the dynamics are governed by those associated with the single pulse until the distance between individual pulses is reduced to one or two sites.

3.5 | Spectral stability

We have proven stable fronts and pulses exists for small ϵ_1 for the 1D model Equation (8). We now remove the assumption that ϵ_1 is small, and assume that a stable front/pulse exists for (8). On doing so, we now consider the spectral stability for the original 2D model Equation (8).

As the 1D solution is stable, the spectrum for the associated linearized self-adjoint operator, $\mathcal{L}_{1D}$, is strictly negative, so

$$\langle \mathcal{L}_{1D} v_j, v_j \rangle < 0. \tag{12}$$

For the 2D problem, the self-adjoint linearized operator has the form,

$$\mathcal{L}_{2D} = \mathcal{L}_{1D} + 2(1+A)\epsilon_1 U_j(1-U_j)\Delta_k.$$

Using a Fourier decomposition for the eigenfunctions in the transverse direction

$$v_{jk} \mapsto v_j e^{i\xi k}, \quad -\pi \le \xi < \pi,$$

we find

$$\mathcal{L}_{2D} v_{jk} = \left[\mathcal{L}_{1D} - 4(1+A)\epsilon_1(1-\cos(\xi))U_j(1-U_j)\right] v_j e^{i\xi k}.$$

As the second term in the sum is a nonpositive operator, by using the inequality (12) we can conclude

$$\langle \mathcal{L}_{2D} v_{jk}, v_{jk} \rangle < 0.$$

Consequently, all the eigenvalues for this operator must be strictly negative.

Lemma 1. *A spectrally stable front/pulse for the 1D problem (10) is spectrally stable for the full 2D problem (8).*

4 | SPOTS: A CASE STUDY

We now consider the existence and spectral stability of spots. A spot is a contiguous set of sites on the lattice that all share language U (or V). All other sites share language V (or U). For example, a 2×3 spot will be a rectangle of height 2 and length 3, so there will be 6 total sites that share language U. When $\epsilon_1 = 0$, a stable spot of any size and shape can be formed. By the Implicit Function Theorem, the spot will persist and be spectrally stable for small ϵ_1. Our goal here is to construct a snaking diagram associated with a particular spot, and then briefly discuss the dynamics as a function of the prestige associated with small perturbations of the steady-state solution.

4.1 | Existence

Consider the snaking diagram associated with a steady-state solution. We will start with the configurations at $R_1 = 0.1$ of a 1×1 square of U sitting on a background of V. The results are plotted in Figure 9. The figure on the left gives the snaking diagram, and some stable solutions arising from the snaking are given on the right. For the snaking diagram stable solutions are marked with a (blue) square, and unstable solutions are marked with a (red) dot. The initial 1×1 configuration grows in norm seemingly without bound until the entire lattice is filled with U. Although we do

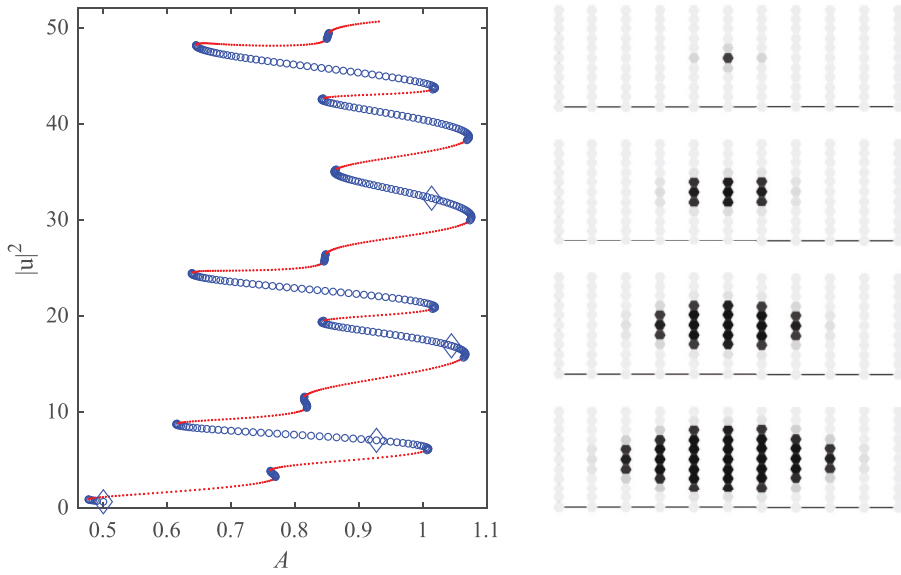

FIGURE 9 The numerically generated snaking diagram starting with a 1×1 spot for a square lattice of size 20×20 when $R_1 = 0.1$. The figure on the left is the snaking diagram, and the figures on the right provide stable solutions arising from the diagram. The notation on the vertical axis, $|u|^2$, represents the square of the ℓ^2-norm of the solution. The upper right panel has $(A, |u|^2) \sim (0.5, 0.6139)$, the next one down has $(A, |u|^2) \sim (0.9276, 7.0127)$, the third one down has $(A, |u|^2) \sim (1.0449, 16.8568)$, and the bottom panel on the right has $(A, |u|^2) \sim (1.0139, 32.2287)$. Each of these points is marked by a large (blue) diamond on the snaking diagram. For the snaking diagram stable, solutions are marked by a (blue) circle, and unstable solutions are marked with a (red) dot. Although we do not show it here, the growth in terms of the total number of contiguous groups holding language U appears to have no upper bound

not provide all the pictures here, as the norm of the solution grows the shape of the contiguous U speakers for a stable solution is either a square or something that has roughly a circular geometry. Regarding the transition from stable to unstable solutions, it is generally not a saddle-node bifurcation, for example, at the transition point the number of unstable eigenvalues will go from zero to two. Moreover, within the curve of unstable solutions, there are additional bifurcations where the number of positive eigenvalues either increases or decreases. The solution structure is rich, but we leave a detailed look at it for a different paper.

It is not necessary that a snaking diagram for a spot connect stable solutions with arbitrarily large norm. For an example, consider the stable solution given in the right panel of Figure 10. The panel on the left shows the associated snaking diagram. Note that there is only one stable branch of solutions associated with this curve. The solution is shown for $R_1 = 0.06$; however, it is not robust relative to large changes in ϵ_1, and it ceases to exist for $R_1 > 0.07$.

Remark 6. We should point out that as in the case of single stripes being concatenated to form more complicated stripe patterns, we can concatenate single spots to form more complicated structures. All that is required for each spot to essentially be an isolated structure is for the spots to be sufficiently separated. Our experience is that a minimal separation distance between two adjacent spots of three sites is enough.

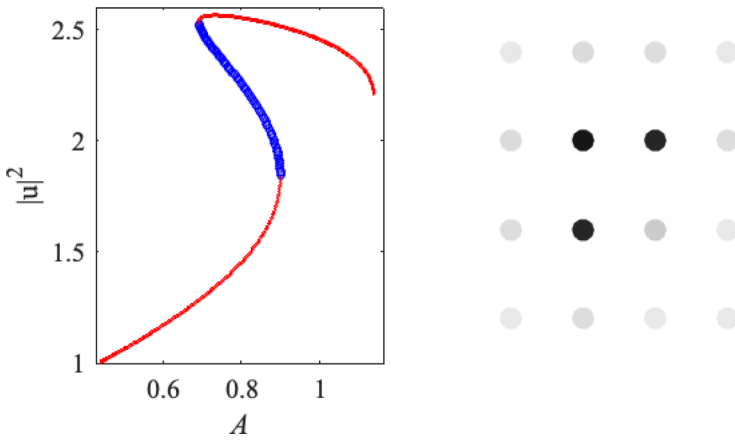

FIGURE 10 A snaking diagram for a spot when $R_1 = 0.06$. The left panel shows the numerically generated diagram, and a representative stable solution is given in the right panel. Stable solutions are marked with a (blue) circle, and unstable solutions are denoted by a (red) dot

4.2 | Dynamics

Now let us consider the dynamical implications of the snaking diagram. In particular, we shall look at the effect of varying A for fixed $R_1 = 0.1$. Recall that for stripes we saw in 3.2 that outside the snaking diagram traveling waves would appear; in particular, if $A < A_-$, then language U would invade language V, whereas if $A > A_+$, then language V would invade language U. Consequently, we expect a similar behavior for spots; in particular, a spot will grow or die as a function of the prestige. For a particular example, we start with a stable solution arising from the 1×1 initial configuration when $A = 0.8165$. The square of the ℓ^2-norm of this solution is roughly 11. This solution is contained in the small stable branch shown in Figure 9 with $A_- \sim 0.8139$ and $A_+ \sim 0.8192$.

First suppose that $A = 0.6 < A_-$. When looking at the snaking diagram, we see that there are no stable steady-state solutions with larger norm for this value of A. The time evolution associated with this initial condition is provided in Figure 11. Of particular interest is the evolution of the square of the norm in the far right panel. We see that the norm is growing up to at least $t = 50$. Although we do not show it here, the norm continues to grow until all the nodes share the common language U. The growth in language U is manifested in the square becoming larger and larger as those nodes containing V at the boundary between U and V switch to language U.

Next suppose that $A = 0.75 < A_-$. When looking at the snaking diagram, we see there is a (stable) steady-state solution with this value of A and which also has a larger norm. The time evolution associated with this initial condition is provided in Figure 12. Of particular interest is the evolution of the square of the norm in the far right panel, which in this case achieves a steady-state. The final state at $t = 50$ corresponds to the first stable solution on the snaking diagram where $A = 0.75$, and whose norm is greater than 11. Language U invades language V until a steady-state configuration is reached.

For the next example, suppose that $A = 0.9 > A_+$. When looking at the snaking diagram, we see there is a steady-state solution with this value of A and which also has a smaller norm. The time evolution associated with this initial condition is provided in Figure 13. Of particular interest is the evolution of the square of the norm in the far right panel, which in this case also achieves a steady-state. The final state at $t = 50$ corresponds to the first stable solution on the snaking diagram where $A = 0.9$, and whose norm is less than 11. Language V invades language U until a steady-state configuration is reached.

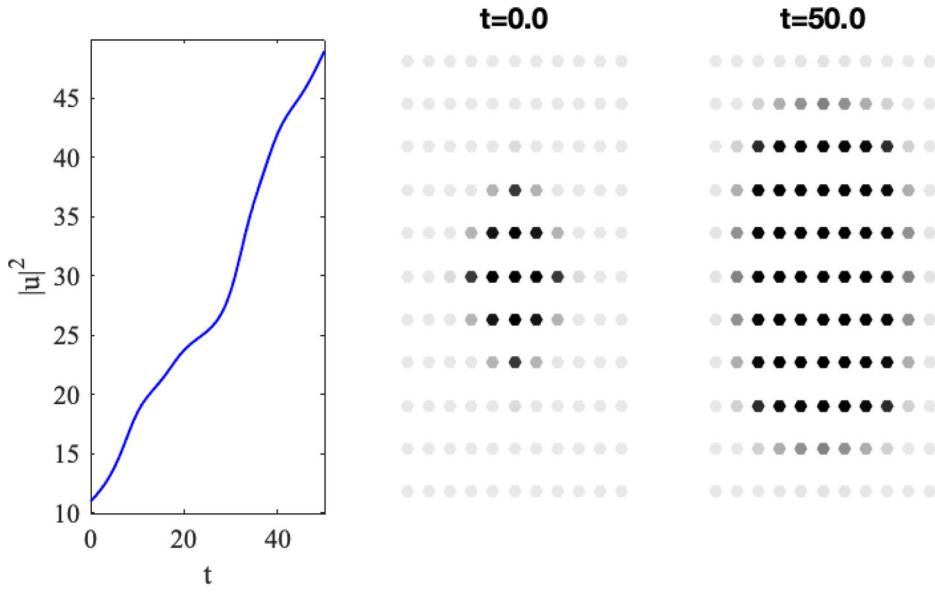

FIGURE 11 The time evolution of an $A = 0.8165$ solution when $A = 0.6$. The panel on the far left shows the evolution of the square of the ℓ^2-norm of the solution

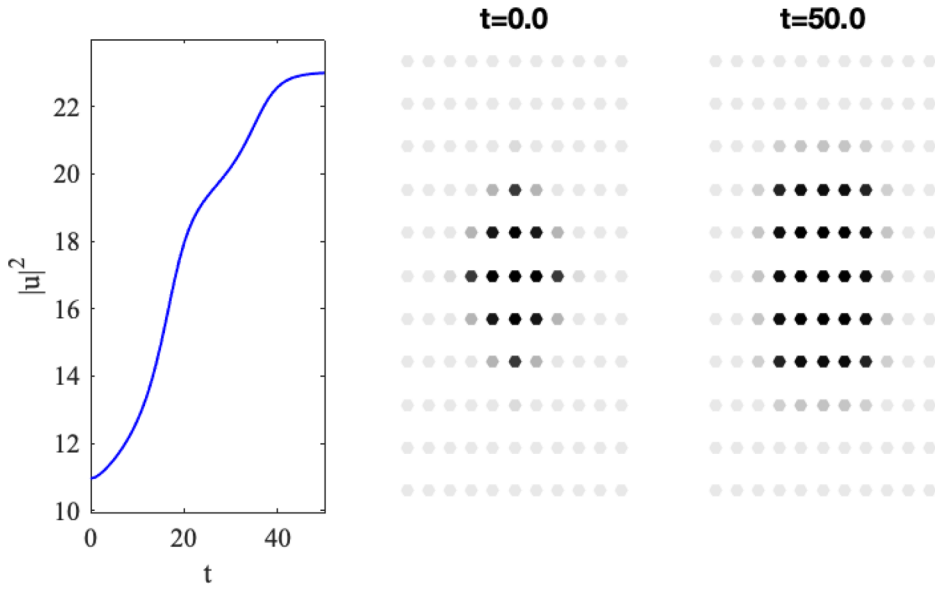

FIGURE 12 The time evolution of an $A = 0.8165$ solution when $A = 0.75$. The panel on the far left shows the evolution of the square of the ℓ^2-norm of the solution

For the last example, suppose that $A = 1.1 > A_+$. When looking at the snaking diagram, we see there is no steady-state solution with this value of A and which also has a smaller norm. The time evolution associated with this initial condition is provided in Figure 14. Of particular interest is the evolution of the square of the norm in the far right panel, which in this case goes to zero. Language V invades language U until the entire lattice shares the common language V.

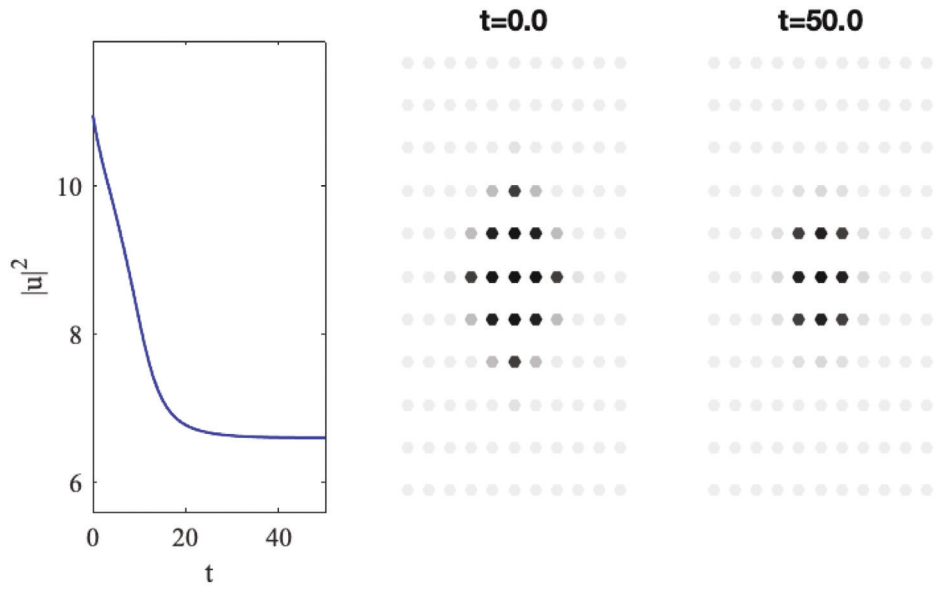

FIGURE 13 The time evolution of an $A = 0.8165$ solution when $A = 0.9$. The panel on the far left shows the evolution of the square of the ℓ^2-norm of the solution

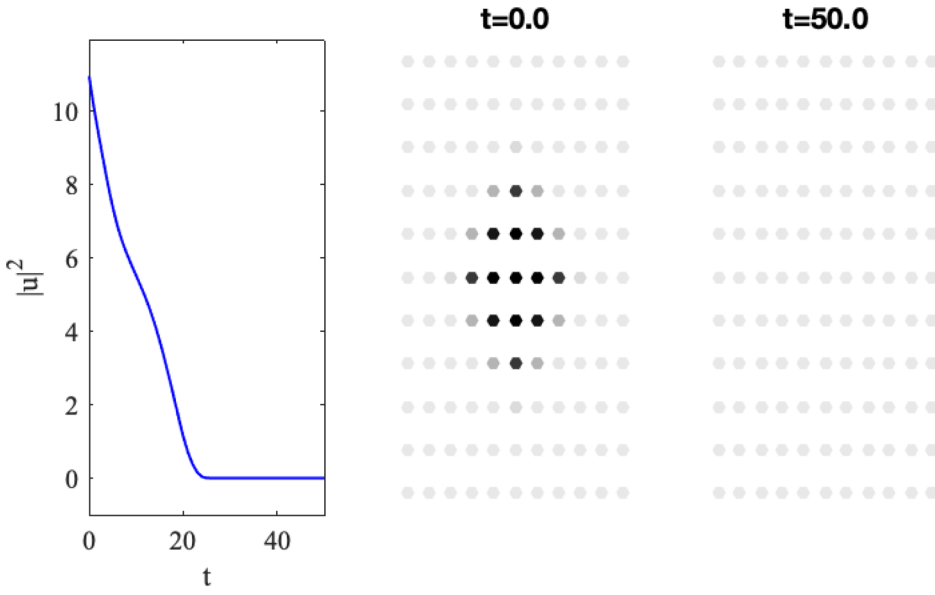

FIGURE 14 The time evolution of an $A = 0.8165$ solution when $A = 1.1$. The panel on the far left shows the evolution of the square of the ℓ^2-norm of the solution

In conclusion, we have the following rule-of-thumb if the initial configuration is near a steady state solution. If the value of A is decreased, so that the prestige of language U increases, then a spot of U in a sea of V will grow until a stable steady-state associated with that value of A is achieved. If no such steady-state exists, then eventually the entire lattice will share language U. On the other hand, if the value of A is increased, so that the prestige of language V increases, then

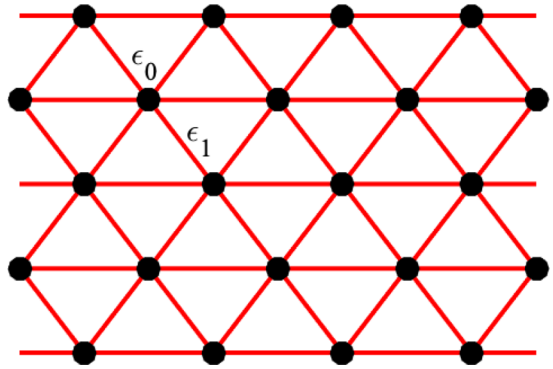

FIGURE 15 The triangular lattice. Each site is connected with equal interaction strength, ϵ_1, to its six nearest neighbors. The on-site interaction rate is ϵ_0

a spot of U in a sea of V will shrink in size until a stable steady-state associated with that value of A is achieved. If no such steady-state exists, then eventually the entire lattice will share language V. Although we do not show it here, this rule was manifested in every numerical simulation that we performed. It would be most interesting to translate this observation into a precise mathematical statement. This is left as an interesting direction for future work.

5 | THE TRIANGULAR LATTICE: A BRIEF LOOK

We now briefly consider the existence problem on a triangular lattice (see Figure 15). As for the square lattice, the on-site interaction strength will be ϵ_0, and the NN strength will be ϵ_1. Again, we will denote $R_1 = \epsilon_1/\epsilon_0$. We will look at fronts and spots for this lattice, and compare the results to those associated with the square lattice.

We first consider the existence of a front. A representative example is given in the left panel of Figure 16. In the right panels of Figure 16 we look at the snaking diagrams for three different values of R_1. When $R_1 = 0.32$ and $R_1 = 0.7$, there are three distinct branches of stable solutions, unlike the square lattice where there is only one branch. The curve of unstable solutions connecting the stable solutions becomes less complicated as R_1 increases. Although we do not show it here, for $R_1 < 0.2$ the bifurcation diagram is very complicated, and there are many branches of stable solutions. Indeed, preliminary calculations seem to suggest that the number of branches becomes arbitrarily large as $R_1 \to 0^+$. For $R_1 \sim 0.7732$, there is a saddle-node bifurcation, and the three branches of stable solutions collapse to one (see the bottom right panel of Figure 16 for $R_1 = 0.85 > 0.7732$). Finally, when compared to the snaking diagram for the front on a square lattice in Figure 2, the prestige interval for which there is a stable stationary front is smaller for the triangular lattice than for the square lattice.

Now consider a spot. We show the snaking diagram (left panel of Figure 17) associated with what for small norm is four contiguous sites speaking the same language (upper right panel of Figure 17). Note that the snaking diagram here is qualitatively similar to that of Figure 9 for a square lattice. In Figure 17, stable solutions marked with a (blue) diamond are plotted in the right panels. The plots on the right have the feature that as A increases, the size of the spot also increases.

Finally, as with the square lattice we note that not all spots grow without bound. Consider the solution given in the right panel of Figure 18, which exists when $R_1 = 0.032$. Here we see

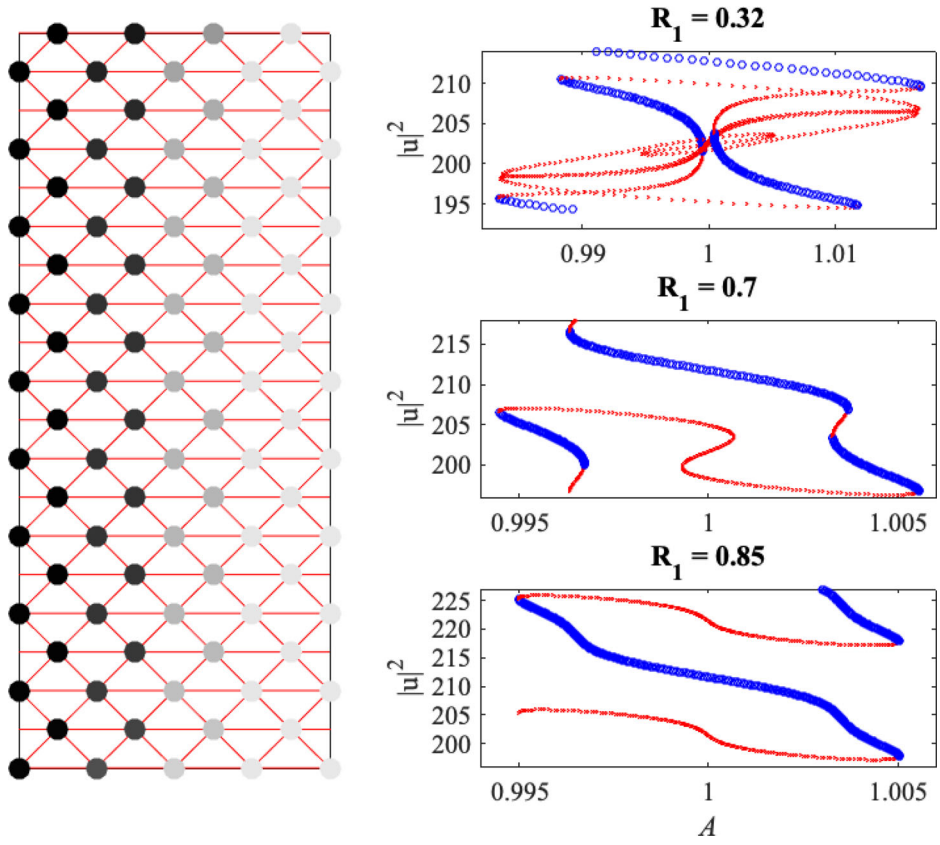

FIGURE 16 The numerically generated snaking diagram for a front on a triangular lattice of size 20×20. The figure on the left is the front, and the figures on the right provide snaking diagrams for three different values of R_1. The notation on the vertical axis, $|u|^2$, represents the square of the ℓ^2-norm of the solution. For the snaking diagram stable, solutions are marked by a (blue) circle, and unstable solutions are marked with a (red) dot. The diagram repeats itself once the entire front has shifted one lattice site

that the snaking diagram does not allow for solutions to get larger and larger in norm, and is instead a bounded curve figure like that in Figure 10 for the square lattice. We numerically find that this solution ceases to exist for $R_1 > 0.035$. It is an interesting problem to determine what initial configurations will lead to snaking diagrams that correspond to solutions that grow in norm until the entire lattice is eventually filled.

6 | EXISTENCE AND SPECTRAL STABILITY OF STRIPES FOR THE CONTINUUM MODEL

We now consider the existence and spectral stability of solutions to the continuum PDE model Equation (9). Although we only derived this model in the context of the square lattice, it also arises for the triangular lattice (in the reaction term R, replace $4\epsilon_1$ with $6\epsilon_1$).

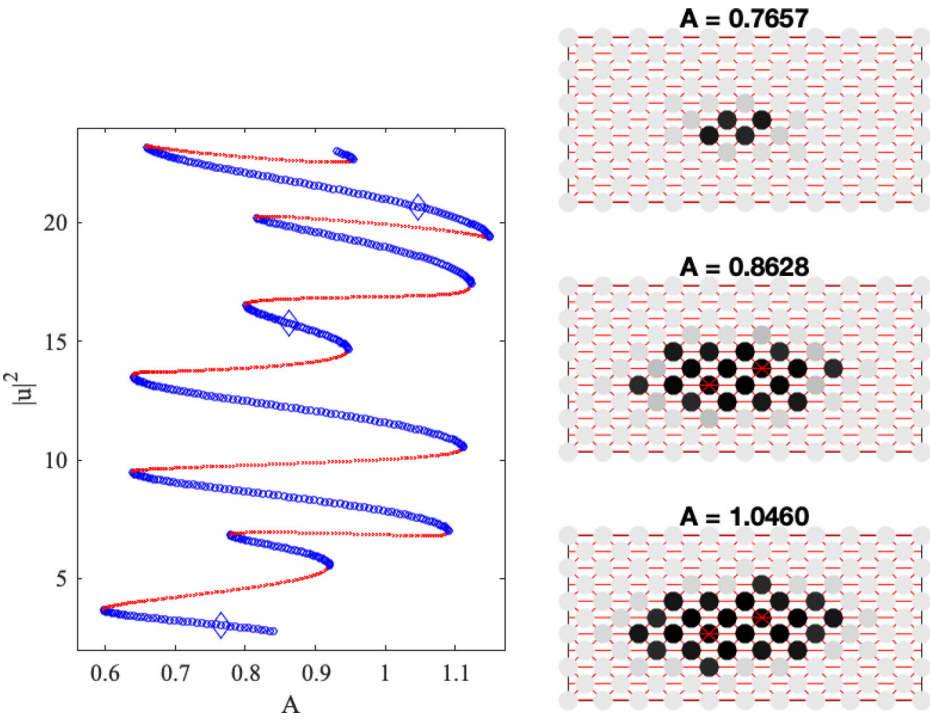

FIGURE 17 The numerically generated snaking diagram for a spot on a triangular lattice of size 20×20 when $R_1 = 0.05$. The figure on the left is the snaking diagram, and the figures on the right provide stable solutions arising from the diagram. The notation on the vertical axis, $|u|^2$, represents the square of the ℓ^2-norm of the solution. The solutions being plotted are marked by a (blue) diamond in the snaking diagram. Stable solutions are marked by a (blue) circle, and unstable solutions are marked with a (red) dot. Although we do not show it here, the growth in terms of the total number of contiguous groups holding language U appears to have no upper bound

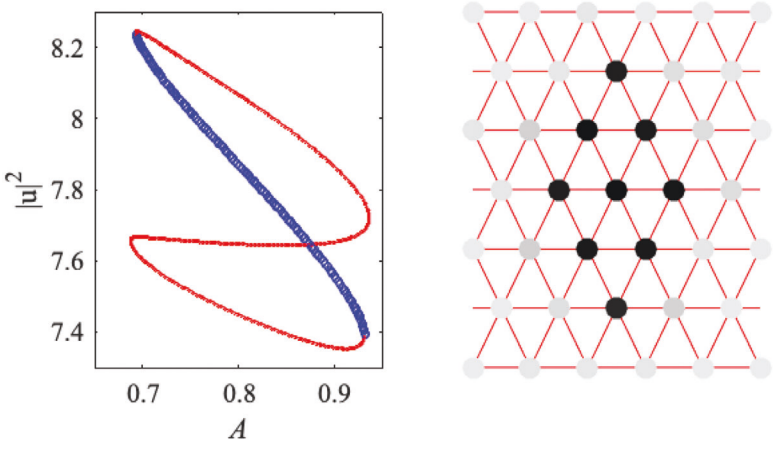

FIGURE 18 A snaking diagram for a spot on a triangular lattice when $R_1 = 0.032$. The left panel shows the numerically generated diagram, and a representative stable solution is given in the right panel

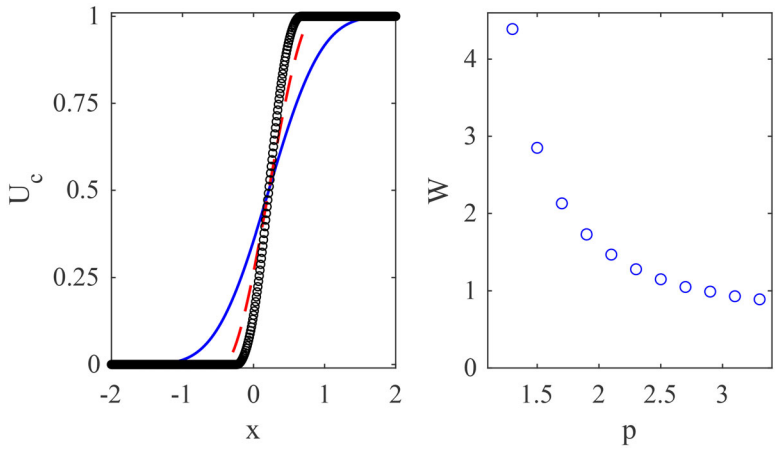

FIGURE 19 The numerically generated compacton fronts for various values of p when $R = 8$. The left panel gives three representative graphs: the solution for $p = 1.3$ is given by the solid (blue) curve, the solution for $p = 2.3$ is given by the dashed (red) curve, and the solution for $p = 3.3$ is given by the black circles. The right panel gives the width of the front, W, for a range of p-values

6.1 | Existence: compactons

The existence problem is settled by finding solutions to the nonlinear ODE (11). Recalling $R = \epsilon_0 + 4\epsilon_1$, under the assumption that neither language is more prestigious, $A = 1$, there exists the exact compacton solution,

$$U_c(x) = \frac{1}{2}\left[1 + \cos\left(\sqrt{\frac{R}{2}}\, x\right)\right].$$

In writing this solutions, there is the implicit understanding that the compacton is continuous with $U_c(x) \equiv 0$ or $U_c(x) \equiv 1$ outside some finite spatial interval. Of course, any spatial translation of the compacton is also a solution. Not only do these compactons define compactly supported pulses, they also define fronts connecting $u = 0$ to $u = 1$. One front satisfies $U_c(x) = 0$ for $x \leq -\pi\sqrt{2/R}$, and $U_c(x) = 1$ for $x \geq 0$ (of course, this front can be translated). Another front satisfies $U_c(x) = 1$ for $x \leq 0$, and $U_c(x) = 0$ for $x \geq \pi\sqrt{2/R}$ (again, this front can be translated). Note that the width of the front/pulse depends on the reaction rate, R.

Remark 7. There is also an explicit compact solution when $p = 3$,

$$U_c(x) = \frac{1}{2}\left[1 + \cos\left(\sqrt{\frac{2R}{3}}\, x\right)\right].$$

Numerically, as illustrated in Figure 19 we see compacton fronts for any $p > 1$. The left panel shows representative solutions, while the right panel gives the width, W, of the compactons for various values of p. Numerically, we see that W is a monotone decreasing function of p.

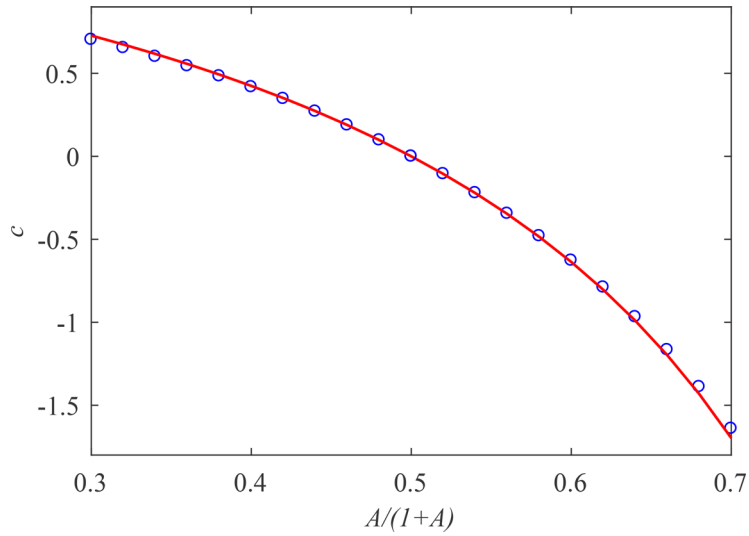

FIGURE 20 The numerically generated wave speed for the $V \to U$ front. The solid (red) curve corresponds to the analytic prediction, and the (blue) circles are the approximate wave speed derived from a numerical simulation of the PDE Equation (14) with $R = 8$ using the standard second-order finite difference schemes to approximate the spatial derivatives

6.2 | Traveling waves

If $A \neq 1$, numerical simulations indicate that the compacton fronts will travel at a constant speed that depends on A. Moreover, the simulations suggest that the shape of the front at a fixed time is roughly that of the compacton for $A = 1$. In order to derive an approximate analytic expression for the wavespeed, we plug $U_c(x + ct)$ into the PDE (14), multiply the resultant equation by $\partial_x U_c(x + ct)$, and then integrate over the domain where the front is nonconstant. Doing all this leads to the following predictions for the wave-speed,

$$V \to U,\ c = -\frac{\sqrt{2R}}{\pi}(A-1); \quad U \to V,\ c = \frac{\sqrt{2R}}{\pi}(A-1). \tag{13}$$

The notation $j \to k$ corresponds to the front that has value j for $x \ll 0$ and value k for $x \gg 0$. See Figure 20 for the comparison of the theoretical prediction with the results of a numerical simulation of the PDE (14). Numerical simulations indicate that these are good predictions for a relatively large range of A for the 1D PDE model; recall the relevant discussion also in Figure 3. Moreover, we find that for R sufficiently large, and away from the saddle-node bifurcation points, these are also good predictions for the wave-speed for the discrete model.

Remark 8. If $A < 1$, so that language U is preferred, the front will move so that language U invades language V. On the other hand, if $A > 1$, so that V is preferred, V will invade U. The standing compacton that exists for $A = 1$ is then seen as a transition between these two invasion fronts.

6.3 | Spectral stability: one dimension

Let us now consider the spectral stability of these compactons. The 1D version of the PDE (9) is

$$\partial_t u = Ru(1-u)[(1+A)u - A] + (1+A)u(1-u)\partial_x^2 u + [1-(1+A)u](\partial_x u)^2. \tag{14}$$

Writing $u = U_{\rm s} + v$, where $U_{\rm s}$ is a steady-state solution, when $A = 1$ the linearized problem for v is

$$\partial_t v = 2\partial_x[U_{\rm s}(1-U_{\rm s})\partial_x v] + g(U_{\rm s})v, \tag{15}$$

where

$$g(U_{\rm s}) = R(-6U_{\rm s}^2 + 6U_{\rm s} - 1) + 2(1-2U_{\rm s})\partial_x^2 U_{\rm s} - 2(\partial_x U_{\rm s})^2.$$

The associated spectral problem is

$$2\partial_x[U_{\rm s}(1-U_{\rm s})\partial_x v] + g(U_{\rm s})v = \lambda v.$$

This is a degenerate Sturm–Liouville problem.

We first consider the spectral stability of fronts. Without loss of generality, assume the solution in question is the $V \to U$ front,

$$U_{\rm s}(x) = \begin{cases} 0, & x \le -\pi\sqrt{2/R} \\ U_{\rm c}(x), & -\pi\sqrt{2/R} < x < 0 \\ 1, & x \ge 0. \end{cases}$$

Lemma 2. *The front is spectrally stable.*

Proof. Outside the interval $[-\pi\sqrt{2/R}, 0]$, the spectral problem is

$$\lambda v = -Rv \quad \rightsquigarrow \quad \lambda = -R, \text{ or } v \equiv 0.$$

Because of the degeneracy associated with the diffusion coefficient, the essential spectrum for the operator comprises a single point.

Over the interval on which the front is nontrivial, $x \in [-\pi\sqrt{2/R}, 0]$, the spectral problem is the singular Sturm–Liouville problem,

$$\frac{1}{2}\partial_x\left[\sin^2\left(\sqrt{\frac{R}{2}}\,x\right)\partial_x v\right] - \frac{R}{4}\left(3\cos^2\left(\sqrt{\frac{R}{2}}\,x\right) - 1\right)v = \lambda v. \tag{16}$$

The form of the coefficients follows from using the analytic expression for the compacton. If $\lambda \neq -R$, then for the sake of continuity we need Dirichlet boundary conditions at the endpoints,

$$v\left(-\sqrt{\frac{2}{R}}\,\pi\right) = v(0) = 0.$$

Due to spatial translation, a solution when $\lambda = 0$ is $v_0(x) = \partial_x U_s$. As the front is monotone, this eigenfunction is of one sign. Consequently, by classical Sturmian theory, $\lambda = 0$ is the largest eigenvalue. ■

Now consider the concatenation of fronts. As each front is a compacton, there will be no tail–tail interaction leading to small eigenvalues. Consequently, each front will add another eigenvalue associated with the eigenvalue of the original front. The associated eigenfunction will simply be a spatial translation of the associated eigenfunction of the original front. In particular, if there are N fronts, then $\lambda = 0$ will be a semi-simple eigenvalue with geometric multiplicity N, and all other eigenvalues will be strictly negative. The multiplicity follows from the fact that each front can be spatially translated without affecting any of the other fronts. We now have:

Corollary 1. *The concatenation of fronts is spectrally stable. Moreover, the zero eigenvalue will have geometric multiplicity equal to the number of concatenated fronts.*

Finally, consider the spectral stability of the pulse compacton,

$$U_c(x) = \frac{1}{2}\left[1 + \cos\left(\sqrt{\frac{R}{2}}\, x\right)\right], \quad -\sqrt{\frac{2}{R}}\,\pi \le x \le \sqrt{\frac{2}{R}}\,\pi.$$

If we start with the concatenation of a left front and a right front, we have a a flat-topped compacton. By Corollary 1 there will be two zero eigenvalues, and the rest of the spectrum will be negative. At the limit of a zero length top we recover the pulse compacton. Consequently, we can think of the pulse as the concatenation of two fronts, a left front and a right front. The eigenvalue at zero will have geometric multiplicity two. One eigenfunction will be $\partial_x U_c$ of the left front, and zero elsewhere, while another will be $\partial_x U_c$ of the right front, and zero elsewhere. Using linearity, we note that one eigenfunction is the sum of these two, which is precisely the expected spatial translation eigenfunction of the full compacton, $\partial_x U_c$.

Corollary 2. *Pulse compactons are spectrally stable, and the zero eigenvalue has geometric multiplicity two.*

6.4 | Spectral stability: two dimensions

For the 1D model Equation (14), a single front is spectrally stable with a simple zero eigenvalue, and a concatenation of N fronts is spectrally stable with a semi-simple zero eigenvalue of multiplicity N. Let $U(x)$ represent a spectrally stable concatenation of N fronts, which is a stripe pattern on the plane. We now consider the spectral stability of the stripes for the full 2D problem.

Lemma 3. *A stripe is spectrally stable.*

Proof. Denote the 1D self-adjoint linearization in (15) about the concatenation as $\mathcal{L}_1$. The linearization about this striped pattern for the full PDE (9) is

$$\mathcal{L}_2 = \mathcal{L}_1 + 2U(1-U)\partial_y^2,$$

which is also self-adjoint. Using the Fourier transform to write candidate eigenfunctions,

$$w(x,y) = v(x)e^{i\xi y},$$

we have,

$$\mathcal{L}_2 w = \big(\mathcal{L}_1 - 2\xi^2 U(1-U)\big)ve^{i\xi y}.$$

We already know $\mathcal{L}_1$ is a nonpositive self-adjoint operator. As $\xi^2 U(1-U) \geq 0$, we can therefore conclude $\mathcal{L}_2$ is a nonpositive self-adjoint operator. In particular, there are no strictly positive eigenvalues. ■

7 | CONCLUSIONS & FUTURE CHALLENGES

We have derived an ODE model of language dynamics on a square lattice (and briefly, a triangular lattice) that is a natural generalization of the AS language model on one lattice site. The model can also be used to discuss, for example, the spread of an opinion through the lattice, or the growth/decay of religious observance on the lattice. We also looked at the continuum limit of the lattice ODE, which is a PDE that features a degenerate diffusion term. We numerically studied the existence of special spatial structures on the lattice; primarily, stripes and spots. Through a combination of numerics and analysis we analyzed the dynamics associated with small perturbations of these spatial structures. Finally, we provided rules-of-thumb to help understand how languages die and grow as a function of their prestige, and interaction with neighboring communities.

As is already evident from the discussion above, there are numerous directions in this emerging field that are worthwhile of further study. Some are already concerning the model at hand. As highlighted earlier, features such as the bifurcation of traveling solutions from standing ones and their scaling laws, or the more precise identification of the discrete solutions and their tails from a mathematical analysis perspective would be of interest. Although it is unclear whether something analytical can be said about the bifurcation diagram of genuinely two-dimensional states such as spots, our numerical observations regarding the model dynamics formulate a well-defined set of conjectures regarding the fate of a spot when the prestige is decreased or increased that may be relevant to further explore mathematically.

It would also be germane to consider variations of the model. Here, we selected as a first step of study to explore an ordered two-dimensional square lattice. However, it is also worth generalizing to more complex networks and modified (influence or) "adjacency matrices" to explore their impact on the findings presented in this work. As indicated herein, the role of near-neighbor interactions is expected to maintain some of the key features we considered; yet, in a progressively connected world the consideration of nonlocal long-range interactions may be of interest in its own right. For example, preliminary results indicate that for a fully connected network it only takes a small level of interaction between adjacent sites before the entire network speaks one language. Another possibility is to insert a spatially heterogeneous prestige A_{jk} and examine how its spatial variation may influence standing and traveling structures. There are numerous variants that can be considered thereafter, for example, how does a local prestige variation interact with the traveling wave patterns discussed in this paper? Such queries have been considered in other contexts where the interactions bear a linear component recently, for example, see Ref. 14,

but have yet to be considered in a fully nonlinear setting such as the one herein. Such studies, as applicable, will be reported in future publications.

Remark 9. The recent work of Kusdiantara and Susanto[20] came to our attention after this paper was accepted for publication. These authors consider the existence and stability of fronts, stripes, and spots for a discrete Allen–Cahn equation on a lattice with a bistable nonlinearity. They consider square, triangular, and honeycomb lattices. Unlike this paper, the coupling between NN sites is assumed to be linear; moreover, it is weak ($R_1 \ll 1$ in our language). Like us, they find that the lattice type does not seem to have a significant influence on the qualitative features of a snaking diagram. It is an interesting problem to consider the model presented in this paper in the small coupling limit, and attempt to determine if nature of the coupling (linear vs. nonlinear) has a significant influence on the snaking diagram. Preliminary calculations indicate it may; especially, when considering the triangular lattice.

ACKNOWLEDGMENT

The work of P. Keverkidis was partially supported by the US National Science Foundation under Grant No. DMS-1809074.

REFERENCES

1. Abrams D, Strogatz S. Modelling the dynamics of language death. *Nature*. 2003;424:900.
2. Abrams D, Yaple H, Wiener R. Dynamics of social group competition: modeling the decline of religious affiliation. *Phys Rev Lett*. 2011;107:088701.
3. Amano T, Sandel B, Eager H, et al.. Global distribution and drivers of language extinction risk. *Proc R Soc B*. 2014;281:20141574.
4. Anderson T, Faye G, Scheel A, Stauffer D. Pinning and unpinning in nonlocal systems. *J Dyn Diff Eq*. 2016;28:897-923.
5. Bramburger J, Sandstede B. Localized patterns in planar bistable weakly coupled lattice systems. *Nonlinearity*. 2020a;33:3500-3525.
6. Bramburger J, Sandstede B, Spatially localized structures in lattice dynamical systems. *J Nonlinear Sci*. 2020b;30:603-644.
7. Bujalski J, Dwyer G, Kapitula T, et al.. Consensus and clustering in opinion formation on networks. *Phil Trans R Soc A*. 2018;376:20170186.
8. Colucci R, Mira J, Nieto J, Otero-Espinar M. Coexistence in exotic scenarios of a modified Abrams-Strogatz model. *Complexity*. 2014;21(4):86-93.
9. Colucci R, Mira J, Nieto J, Otero-Espinar M. Non trivial coexistence conditions for a model of language competition obtained by bifurcation theory. *Acta Appl Math*. 2016;146:187-203.
10. Dhooge A, Govaerts W, Kuznetsov Y. Matcont: a MATLAB package for numerical bifurcation analysis of ODEs. *ACM TOMS*. 2003;29:141-164.
11. Eekhoff K. Opinion formation dynamicswith contrarians and zealots. *SIAM Undergraduate Res. Online*. 2019;12.
12. Elmer C, Van Vleck E. A variant of Newton's method for the computation of traveling waves of bistable differential-difference equations. *J Dyn Diff Eq*. 2002;14(3):493-517.
13. Fujie R, Aihara K, Masuda N. A model of competition among more than two languages. *J Stat Phys*. 2013;151:289-303.
14. Hoffman A, Hupkes H, Van Vleck E. *Entire Solutions for Bistable Lattice Differential Equations with Obstacles*. American Mathematical Society; 2017.
15. Hupkes H, Verdun Lunel S. Analysis of Newton's method to compute travelling waves in discrete media. *J Dyn Diff Eq*. 2005;17(3):523-572.
16. Hupkes H, Sandstede B. Stability of pulse solutions for the discrete Fitzhugh-Nagumo system. *Trans Amer Math Soc*. 2013;365:251-301.

17. Hupkes H, Pelinovsky D, Sandstede B. Propagation failure in the discrete Nagumo equation. *Proc Amer Math Soc*. 2011;139(10):3537-3551.
18. Juane M, Seoane L, Mu nuzuri A, Mira J. Urbanity and the dynamics of language shift in Galicia. *Nature Comm*. 2019;10:1680.
19. Kevrekidis P, Kevrekidis I, Bishop A. Propagation failure, universal scalings and Goldstone modes. *Phys Lett A*. 2001;279(5-6):361-369.
20. Kusdiantara R, Susanto H. Snakes in square, honeycomb, and triangular lattices. *Nonlinearity*. 2019;32:5170-5190.
21. Marvel S, Hong H, Papush A, Strogatz S. Encouraging moderation: clues from a simple model of ideological conflict. *Phys Rev Lett*. 2012;109:118702.
22. Mira J, Paredes Á. Interlinguistic similarity and language death dynamics. *Europhys Lett*. 2005;69(6):1031-1034.
23. Mira J, Seoane L, Nieto J. The importance of interlinguistic similarity and stable bilingualism when two languages compete. *New J Phys*. 2011;13:033007.
24. Moore R, Promislow K. Renormalization group reduction of pulse dynamics in thermally loaded optical parametric oscillators. *Physica D*. 2005;206:62-81.
25. Otero-Espinar M, Seoane L, Nieto J, Mira J. An analytic solution of a model of language competition with bilingualism and interlinguistic similarity. *Physica D*. 2013;264:17-26.
26. Parker R, Kevrekidis P, Sandstede B. Existence and spectral stability of multi-pulses in discrete Hamiltonian lattice systems. *Physica D*. 2020;408:132414.
27. Promislow K. A renormalization method for modulational stability of quasi-steady patterns in dispersive systems. *SIAM J Math Anal*. 2002;33(6):1455-1482.
28. Sandstede B. Stability of multiple-pulse solutions. *Trans Amer Math Soc*. 1998;350:429-472.
29. Sandstede B. Stability of travelling waves. In Fiedler B, ed. *Handbook of Dynamical Systems*. Elsevier Science; 2002:983-1055.
30. Stauffer D, Castelló X, Eguíluz V, San Miguel M. Microscopic Abrams-Strogatz model of language competition. *Physica A*. 2007;374:835-842.
31. Tanabe S, Masuda N. Complex dynamics of a nonlinear voter model with contrarian agents. *Chaos*. 2013;23:043136.
32. Vazquez F, Castelló X, San Miguel M. Agent based models of language competition: macroscopic descriptions and order-disorder transitions. *J Stat Mech*. 2010:P04007.
33. Vidal-Franco I, Guiu-Souto J, Mu nuzuri A. Social media enhances languages differentiation: a mathematical description. *R Soc Open Sci*. 2017;4:170094.
34. Wang S, Rong L, Wu J. Bistability and multistability in opinion dynamics models. *Appl. Math Comp*. 2016;289:388-395.
35. Yun J, Shang SC, Wei XD, Liu S, Li ZJ. The possibility of coexistence and co-development in language competition: ecology-society computational model and simulation. *SpringerPlus*. 2016;5:855.
36. Zhou Z, Szymanski B, Gao J. Modeling competitive evolution of multiple languages. *PLOS One*. 2020;15(5): e0232888.

How to cite this article: Kapitula T, Kevrekidis PG. Language competition on lattices. *Stud Appl Math*. 2021;1–29. https://doi.org/10.1111/sapm.12439